Fluoroethylene Carbonate Additives to Render Uniform Li Deposits in Lithium Metal Batteries

*Xue-Qiang Zhang, Xin-Bing Cheng, Xiang Chen, Chong Yan, and Qiang Zhang**

Lithium (Li) metal has been considered as an important substitute for the graphite anode to further boost the energy density of Li-ion batteries. However, Li dendrite growth during Li plating/stripping causes safety concern and poor lifespan of Li metal batteries (LMB). Herein, fluoroethylene carbonate (FEC) additives are used to form a LiF-rich solid electrolyte interphase (SEI). The FEC-induced SEI layer is compact and stable, and thus beneficial to obtain a uniform morphology of Li deposits. This uniform and dendrite-free morphology renders a significantly improved Coulombic efficiency of 98% within 100 cycles in a Li | Cu half-cell. When the FEC-protected Li metal anode matches a high-loading $LiNi_{0.5}Co_{0.2}Mn_{0.3}O_2$ (NMC) cathode (12 mg cm^{-2}), a high initial capacity of 154 mAh g^{-1} (1.9 mAh cm^{-2}) at 180.0 mA g^{-1} is obtained. This LMB with conversion-type Li metal anode and intercalation-type NMC cathode affords an emerging energy storage system to probe the energy chemistry of Li metal protection and demonstrates the material engineering of batteries with very high energy density.

1. Introduction

The pursuit of an electrochemical energy storage system with high energy density has never stopped since the first battery was invented by Count Volta in 1800. In the early 1990s, the Sony Corporation commercially introduced a lithium (Li)-ion battery (LIB) based on the use of Li-intercalation graphite anode.[1] As LIB can deliver an energy density of at least 2.5 times higher than that of nickel–cadmium and lead–acid batteries, it realized a great success in portable devices, such as mobile phones and laptops.[2] However, either success or failure of LIB all boils down to graphite anode. The relatively low specific capacity of graphite anode (372 mAh g^{-1}) limits the energy density of LIB to satisfy the demand of modern electric vehicles and wearable devices. Among various anode materials, metallic lithium anode with an extremely high theoretical specific capacity (3860 mAh g^{-1}) and the lowest reduction potential (−3.04 V vs standard hydrogen electrode) has been strongly reconsidered as a promising next-generation anode.[3,4]

Nevertheless, the practical application of Li metal anode is severely hindered by the uncontrollable formation of dendritic and mossy Li on Li anode surface as well as the low Coulombic efficiency during repeated stripping/plating process.[5,6] Li dendrites are generally induced by inhomogeneous distributions of space charge,[7] current density on anode surface,[8] and the crack of solid electrolyte interphase (SEI).[9] During the past several decades, much effort has been devoted to prevent the parasitic growth of Li dendrites in a working battery.[4,5,10,11] Among these strategies, in situ formation of SEI with high uniformity and stability is one of the most effective and convenient routes to suppress Li dendrite growth due to its prominent impact and low cost, particularly in industrial manufacture of batteries.[12] Many electrolyte additives are employed to facilitate the formation of stable SEI layer on Li metal anode, such as vinylene carbonate (VC),[13] fluoroethylene carbonate (FEC),[14,15] $LiNO_3$,[16] Cs^+,[17] Li polysulfide,[18] lithium chloride,[19,20] copper acetate,[21] and highly concentrated electrolyte.[22] Li metal anode with protective SEI layer exhibits a superior cycling performance in high-energy-density Li metal battery (LMB).

Among the LMBs, Li–sulfur (Li—S) and Li–oxygen (Li—O_2) batteries with a high theoretical energy density of 2600 and 3500 Wh kg^{-1} have been strongly explored,[23] while LMB pairing intercalation-type cathode (such as $LiNi_{0.5}Co_{0.2}Mn_{0.3}O_2$ (NMC)) versus Li metal anode is little involved. This NMC-based LMB employs the same cathode with LIB, which is very easy to integrate with the current LIB manufacturing process and further improve the energy density of the current LIB.[24] However, Li deposition behavior has not been understood well in this system. Lu et al. described that when charging LMB with lithium nickel cobalt aluminum oxide cathode versus Li anode at high rate, large dendrites and dead Li formed on the Li metal anode, leading to a large polarization in a working battery.[25] The highly resistive porous dead Li layer dramatically increased the cell impedance and resulted in cell degradation and final failure. To suppress Li dendrite growth in these LMBs, Zheng et al. manipulated the cell operation model at low charge/rapid discharge rate to facilitate the formation of a stable and flexible SEI to suppress Li dendrite growth.[26] However, the mostly applied strategy of electrolyte additives to benefit the formation of robust SEI is rarely employed in the high-energy-density LMB.[27] It is of great significance to clearly demonstrate the Li deposition behavior and investigate the cycling performance of these LMBs in organic electrolytes with additives.

X.-Q. Zhang, X.-B. Cheng, X. Chen,
C. Yan, Prof. Q. Zhang
Beijing Key Laboratory of Green Chemical
Reaction Engineering and Technology
Department of Chemical Engineering
Tsinghua University
Beijing 100084, China
E-mail: zhang-qiang@mails.tsinghua.edu.cn

DOI: 10.1002/adfm.201605989

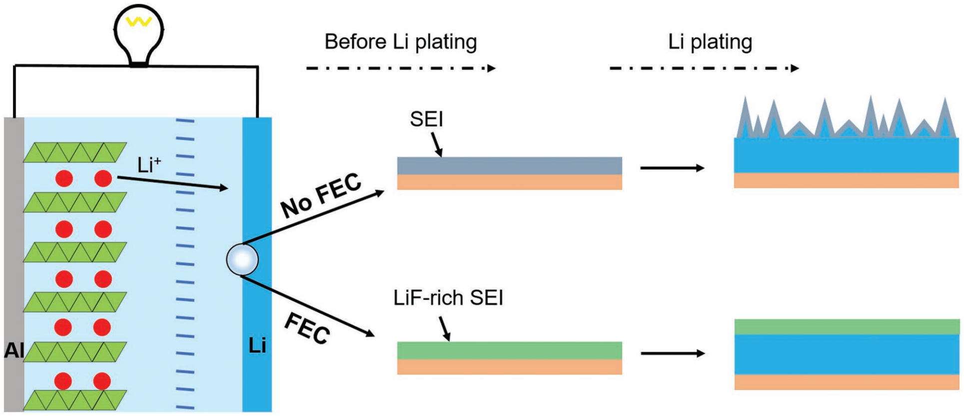

Figure 1. Schematic illustration of the effect of FEC additives on a Li metal anode. The electrolyte is 1.0 M $LiPF_6$ in EC/DEC (1:1 by volume) with/without FEC additives.

Here, we report the use of FEC additives in high-energy-density LMB to protect a Li metal anode (**Figure 1**). The NMC cathode was chosen to match the Li metal anode, which can effectively improve the cathode capacity relative to the conventional oxide cathodes ($LiFePO_4$, $LiCoO_2$, etc.). We primarily verified the hypothesis of LiF-rich SEI induced by FEC additives through first-principles calculations and X-ray photoelectron spectroscopy (XPS). In the Li | Cu half-cell test, we demonstrated a uniform and dense morphology of Li deposits as well as improved cell cycling performance with the presence of FEC. Voltage polarization was greatly reduced and Coulombic efficiency was effectually improved due to the thinner and denser interphase on Li anode. In the Li | NMC cell, a high capacity and long lifespan are achieved for the FEC-protected Li metal anode.

2. Results and Discussion

2.1. FEC-Induced SEI Formation

FEC is beneficial for robust SEI formation on graphite,[28] silicon,[29] and high-voltage cathode.[30,31] To gain the molecular insights into the SEI formation, we first investigated the SEI formation induced by FEC additives in ethylene carbonate (EC)/diethyl carbonate (DEC) by first-principles calculation (**Figure 2**a,b). During cell charging, FEC with lower level of the lowest unoccupied molecular orbital (LUMO) (−0.87 eV) is easier to be reduced than EC (−0.38 eV) and DEC (0 eV) on the surface of Li metal anode (Figure 2b), significantly decreasing the consumption of solvent.

During the FEC-induced SEI formation, the carbon–fluorine bond is first broken around 310 fs (Figure 2c) and the fluorine–lithium distance is near to that in lithium fluoride crystal (0.2032 nm), indicating the generation of LiF on the surface of Li metal anode. The correspondingly proposed reaction mechanism for generation of LiF is shown in Scheme S1 (Supporting Information). The as-obtained LiF is considered as an important SEI component to form the uniform and compact lithium deposits.[15,20] EC solvent can also decompose on the Li surface. However, there is no/less EC decomposition reaction observed on the LiF surface during the same ab initio molecular dynamics (AIMD) (Figure S1, Supporting Information). Therefore, it can be inferred that the LiF products induced by FEC sacrifice act as the protective SEI layer on Li anode. With the FEC-induced SEI protecting Li metal, parasitic reactions between Li and electrolyte are effectively suppressed.

XPS of the anode was conducted to further probe the surface chemistry of FEC-induced SEI layer (**Figure 3** and Figure S2, Supporting Information). A high F content of 10.8 at% is achieved in the FEC electrolyte, which is apparently

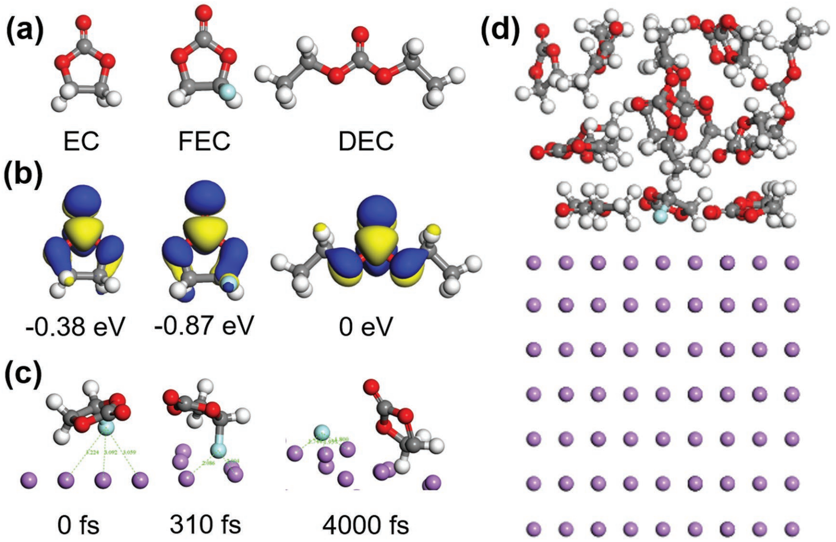

Figure 2. First-principles study of the role of FEC. a) Molecular structure of EC, FEC, and DEC. b) Visual LUMO and corresponding relative energy of EC, FEC, and DEC. c) Ab initio molecular dynamics model. d) Complete sequence of FEC molecule decomposed on Li anode. The hydrogen, lithium, carbon, oxygen, and fluorine atom were marked with white, purple, gray, red, and blue, respectively.

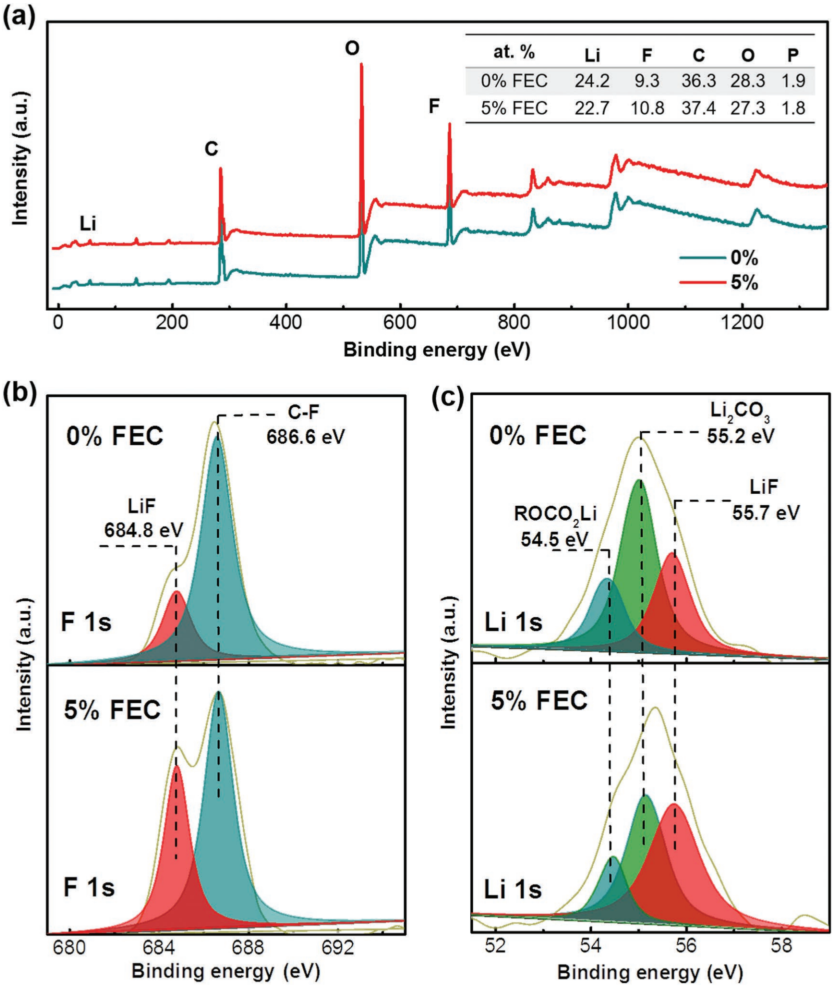

at. %	Li	F	C	O	P
0% FEC	24.2	9.3	36.3	28.3	1.9
5% FEC	22.7	10.8	37.4	27.3	1.8

Figure 3. XPS characterization of the SEI layer. a) XPS spectra of the SEI layer, the inset table: atomic ratio of elements in the SEI layer. b,c) F 1s and Li 1s spectra of the SEI layer induced by 0% and 5% FEC after lithium stripping on Cu substrate after ten cycles.

larger than that of 9.3 at% in FEC-free routine electrolyte (Figure 3a). There are two peaks in the F 1s spectra: LiF at 684.8 eV and C—F bonds at 686.6 eV (Figure 3b). The proportion of LiF in the FEC-containing electrolyte induced SEI layer (48.2%) accounts more than that of in the FEC-free induced SEI layer (29.5%) according to the ratio of peak area. Therefore, more LiF forms in FEC-induced SEI layer than FEC-free induced SEI layer.

The LiF-rich SEI is the product of spontaneous reactions between fresh Li and FEC, instead of the adverse reaction between Li and EC or DEC. LiF is critically important in the formation of stable and uniform SEI to suppress Li dendrite growth.[15,20] On one hand, LiF is a robust electrical insulator ($\approx 10^{-31}$ S cm^{-1}) to prevent electrons from crossing the SEI layer.[32] On the other hand, LiF with a low diffusing energy and high surface energy for Li ions exhibits an overwhelming advantage in enhancing surface diffusion of Li^+ during electrodeposition and directing a uniform and dendrite-free morphology.[20] In Li 1s spectra, a similar result can be reached (Figure 3c). The peak of LiF (55.7 eV) is also enhanced in FEC-induced SEI layer. Consequently, by introducing FEC into the electrolyte, an LiF-rich SEI layer is achieved, which is expected to suppress Li dendrite growth and render a long lifespan of Li metal anode.

2.2. Li | Cu Half-Cell Performance

To evaluate the long-term stability of Li plating/stripping behavior in a working battery, the coin-type Li | Cu half-cells with and without FEC additives in electrolyte were assembled. In order to obtain a stable and low-viscosity electrolyte, the amount of FEC additives in Li hexafluorophosphate ($LiPF_6$)-EC/DEC electrolyte is set as 5% (by volume) in this work. The $LiPF_6$-EC/DEC electrolyte without FEC additive (0% FEC) was also prepared as a control sample.

Coulombic efficiency was employed to indicate Li utilization rate during one Li plating/stripping cycle and calculated by the ratio of the amount of Li stripped and plated on Cu substrate. The Coulombic efficiencies of Li | Cu cells at 0.1 and 0.5 mA cm^{-2} are shown in **Figure** 4a,b, respectively. The initial Coulombic efficiency of cells in 0% and 5% FEC electrolyte is 78% and 90% at 0.1 mA cm^{-2}, respectively, demonstrating a superior role of FEC in constructing a highly efficient SEI (Figure 4a). During 100 cycles (>1000 h), the Coulombic efficiency of 0% FEC electrolyte is evidently lower than 92%, while a remarkably high Coulombic efficiency of 98% is achieved in 5% FEC electrolyte. The superior cycling performance of 5% FEC electrolyte is attributed to the uniform and dendrite-free Li metal protected by the LiF-rich SEI. When the current density is increased to 0.5 mA cm^{-2}, Coulombic efficiencies of 88% and 95% are obtained in 0% and 5% FEC electrolyte (Figure 4b), respectively, further confirming the effective role of FEC-induced LiF-rich SEI at high current density. A 2% FEC electrolyte was also prepared. The Coulombic efficiency of 2% FEC electrolyte is inferior to 5% FEC electrolyte but superior to 0% FEC electrolyte (Figure S3, Supporting Information), which demonstrates that 5% FEC is a better choice for further investigation.

The polarization profiles in different cycles were recorded to gain the kinetic behavior during Li stripping/plating (Figure 4c and Figure S4, Supporting Information). The polarization of 5% FEC electrolyte at 0.5 mA cm^{-2} from the charge/discharge curves is nearly the same, 50 mV at both 10th and 50th cycles, while it is 58 mV at 10th and 72 mV at 50th cycles for 0% FEC electrolyte. The large polarization of 0% FEC electrolyte is caused by the continuous Li dendrite growth. These dendrites result in a highly resistive layer with SEI entangled with dead Li metal, which increases the ion and electron diffusion resistance within the anode matrix. Therefore, the polarization is rising gradually. In contrast, Li anode protected by the LiF-rich SEI

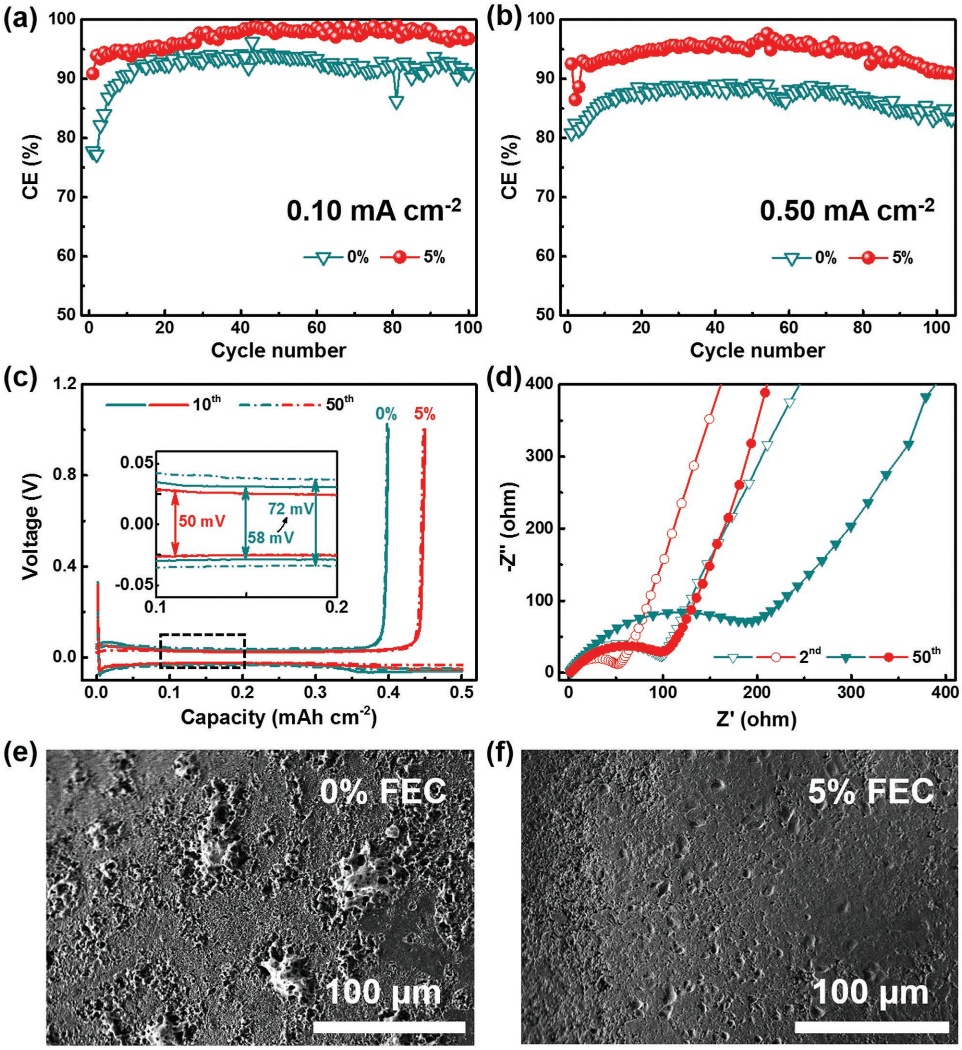

Figure 4. Electrochemical performance and SEM images of Li | Cu cells. Coulombic efficiency (CE) at a current density of a) 0.10 and b) 0.50 mA cm^{-2} with a capacity of 0.5 mAh cm^{-2}. c) Polarization curves of plating/stripping process in (b). d) EIS of Li | Cu cells at frequency ranging from 10^5 to 10^{-1} Hz under amplitude of 10 mV. SEM images of Li depositing morphology on Cu foils after 50 cycles with e) 0% and f) 5% FEC.

exhibits a stable interface and dendrite-free Li depositing morphology, and therefore small and stable overpotential during Li stripping/plating.

Electrochemical impedance spectroscopy (EIS) measurements of Li | Cu half-cells at 0.5 mA cm^{-2} were carried out to reveal the conductivity of SEI on Li metal anode. Nyquist plots of the cells with 0% and 5% FEC are with one semicircle in high frequency (Figure 4d), which is always ascribed to Li$^+$ migration through the SEI on the electrode surface.[33] 5% FEC electrolyte can effectively decrease the SEI resistance at second cycle (60 Ω for 5% FEC electrolyte, 110 Ω for 0% FEC electrolyte), implying high conductivity of Li$^+$ through SEI layer. After 50 cycles, the cell with 5% FEC exhibits evidently lower SEI resistance than that with 0% FEC electrolyte (110 Ω for 5% FEC electrolyte, 250 Ω for 0% FEC electrolyte). Consequently, SEI formed in the FEC electrolyte is more stable and conductive, rendering a high Li-ion conductivity.

After 50 cycles in coin-type Li | Cu half cells, morphologies of Li deposits were recorded (Figure 4e,f and Figure S5, Supporting Information). 0% FEC electrolyte results in an uneven surface and optically visible dead and porous Li on the substrate. When FEC was introduced into the electrolyte, a uniform and smooth surface without any dendrite and porous structure was obtained. The porous and loose layer is mainly composed of deposited Li losing contact with electrons (dead Li).[25,34] For dendritic and nonuniform Li due to the lack of protective SEI, dead Li forms easily during the stripping process. The accumulation of dead Li in repeated plating/stripping process leads to porous and resistive Li films in 0% FEC electrolyte. However, the LiF-rich SEI induced by FEC additives significantly benefits the uniform Li deposits and reduces the formation of dead Li, leading to dense and less resistive deposited Li films.

2.3. Li | NMC Full-Cell Performance

We verified the concept of LMB with intercalation-type NMC cathode and conversion-type Li metal anode. Commercial

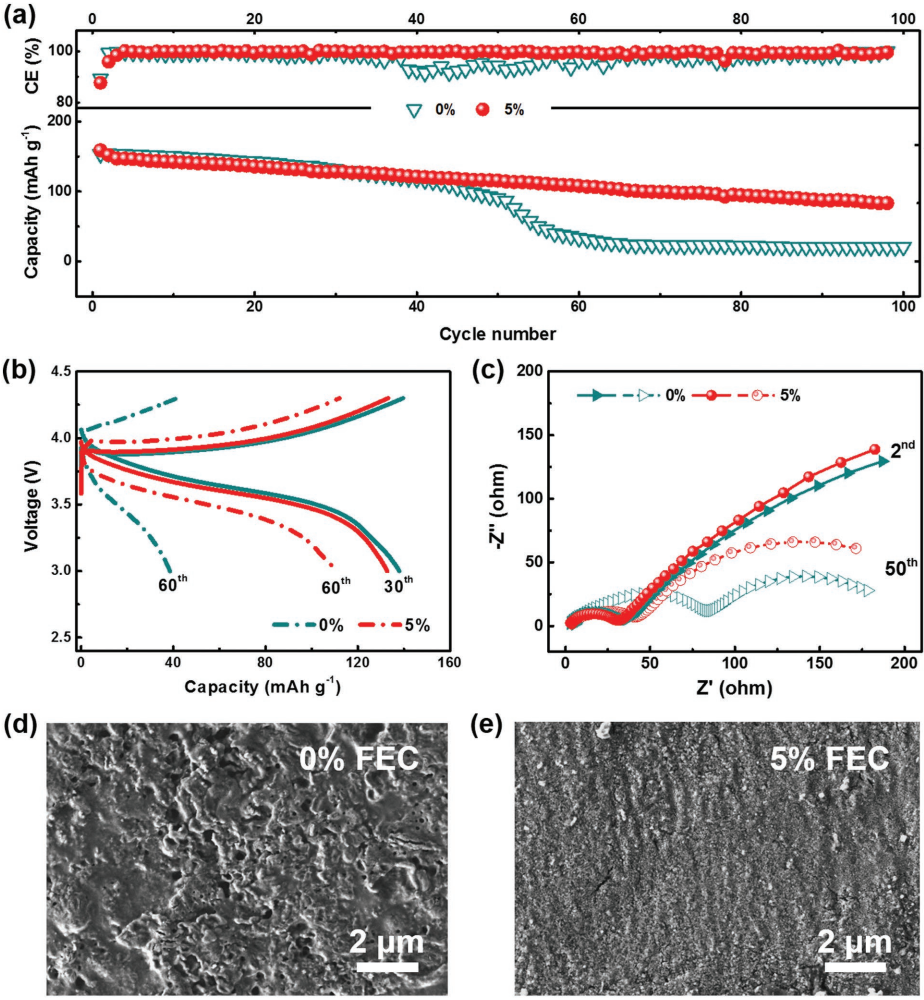

Figure 5. Electrochemical performance and SEM images of Li | NMC cells. a) Cycling performance and b) voltage profiles of cells at 1.0 C, 3.0–4.3 V, with one formation cycle initially performed at 0.1 C prior to 1.0 C cycling. c) EIS of Li | NMC cells after 2 and 50 cycles. SEM images of the Li anode surfaces after Li plating obtained from the Li | NMC cells at 1 C after cycling for 50 cycles with d) 0% and e) 5.0% FEC.

$LiNi_{0.5}Co_{0.2}Mn_{0.3}O_2$ cathode with a very high areal loading of 12–14 mg cm^{-2} was used in this work. Prior to investigating the FEC-protected Li metal, the effect of FEC on high-voltage cathode materials as film-forming additives must be excluded. Cyclic voltammetry (CV) confirms that there are no significant decompositions of FEC in the range of 3.0–4.3 V (Figure S6, Supporting Information).

Figure 5 exhibits the cycling performance of Li | NMC cells with 0% and 5% FEC electrolyte at 1.0 C (1.0 C = 180 mA g^{-1}) after 0.1 C activation for one cycle. All cells deliver nearly the same reversible capacity (154 mAh g^{-1}) and Coulombic efficiency of 99.5% in the initial cycles (Figure 5a). The effect of FEC is not conspicuous in the initial 40 cycles. However, a sharp capacity decay at 40th cycle for 0% FEC is recorded. The precipitous drop in capacity is attributed to the failure of the conductive framework in the anode, which is induced by the highly resistive layer with SEI entangled with dead Li metal. There is no sharp capacity decay in 5% FEC electrolyte, due to the stable LiF-rich SEI and uniform Li deposition contributed by FEC additives. However, there is also a continuous capacity decay for 5% FEC electrolyte (65% retention after 100 cycles). The fading of the capacity in the Li | NMC cells is synergy effects among Li anode, NMC cathode, and organic electrolyte. The charge–discharge voltage profiles at different cycles (Figure 5b) clearly demonstrate the higher capacity retention in 5% FEC electrolyte (65%) than that in 0% FEC electrolyte (14%), indicating FEC is apparently beneficial for the capacity stability of Li | NMC cells.

Figure 5c displays the Nyquist plots of Li | NMC cells. The cells with 0% and 5% FEC electrolyte are with nearly the same resistance (40 Ω) at second cycle. However, with the depth of discharge, the SEI resistance of 0% FEC electrolyte rises to 100 Ω, while that of 5% FEC electrolyte is only 60 Ω after 50 cycles. The ever-increasing resistance indicates the unstable interface and crackly SEI of 0% FEC electrolyte.

To obtain the depositing morphology of Li metal anode in Li | NMC cells, cycled Li anodes were characterized by scanning electron microscopy (SEM) images. As shown in Figure 5d,e, the surface of Li anode (in charged state) in 0% electrolyte is porous and loose, exhibiting the existence of dendrite growth and dead Li, while the surface of cycled Li anode obtained from 5% FEC electrolyte is dense and uniform. The morphology of Li anode in discharged state was also recorded in Figure S7 (Supporting Information). Uniform stripping of Li is observed in 5% FEC electrolyte compared to 0% FEC electrolyte. From the cross-section view of deposited Li, there is a layer consisting of Li participating in cycling (reactive Li) on the top of bulk Li (Figure S8, Supporting Information). A porous and loose dead Li layer induced by dendrite growth results in the formation of a thick reactive Li layer, affording a high Li-ion diffusion resistance in a working cell. The thickness of reactive Li in 5% FEC electrolyte (≈40 µm) is much less than that in 0% FEC electrolyte (≈100 µm). The thinner reactive Li layer in 5% FEC electrolyte indicates the reduction of the formation of dead Li and Li dendrites.

2.4. The Role of FEC on Li Metal Protection

Based on the aforementioned results, it is clearly implied that the FEC-induced SEI is more stable and conductive, promoting the uniform Li stripping and plating and superior long-term cycling performance of Li | NMC cells. Recently, LiF is verified to significantly promote Li-ion diffusion on Li anode/electrolyte interface, which renders the possibility of uniform Li deposition in organic electrolyte.[35] FEC additive, a frequently used electrolyte additive in LIB, is reported to lead to LiF-containing components on graphite,[28,36] silicon anode,[29,37] hard carbon,[38] TiO_2@C anode,[39] Sn—P composite,[40] Sb-based alloys,[41] fluorine-doped Sn—Ni film electrode,[42] Li_xSi_y alloy,[43] Sn,[44] MoS_2-C anode,[45] Mo_6S_8,[46] and so on. FEC is found to effectively enhance the cycling performance of high-voltage Li-ion cells.[30] However, the systematical insight into the effect of FEC additives on in situ formed SEI on the surface of Li metal in LMB (such as Li | NMC cell) is lacking. Moreover, FEC additive is soluble in carbonate electrolyte and easy to process, which circumvents the trouble such as toxicity, corrosion, and insolubility led by HF[47] and solid LiF[20] in practical applications.

Carbonate electrolytes are compatible with high-voltage cathode (such as NMC), however, carbonate electrolytes (such as EC, PC, DMC, etc.) generally exhibit low Coulombic efficiency (≈85%) compared to ether electrolyte.[10,48] The addition of FEC enhances the Coulombic efficiency of carbonate electrolyte. We first verified the hypothesis of the formation of LiF-rich SEI in the presence of FEC additive by first-principles calculation and XPS. FEC with lower LUMO energy is reduced prior to EC and DEC, forming LiF-rich SEI to prevent the reactions between electrolyte and Li metal. Then further researches in Li | Cu cells show that high Coulombic efficiency (≈98%), uniform and dense Li deposits after long cycles in FEC electrolyte are achieved. EIS measurement also demonstrates that the resistance is largely reduced in FEC electrolyte compared to FEC-free electrolyte. These results confirm that the LiF-rich SEI induced by FEC is uniform and conductive for Li-ion diffusion, realizing smooth and dense Li deposits, high Coulombic efficiency, and reduced formation of dead Li.

LMB employing Li metal anode and intercalated cathode (such as NMC) provides more promising opportunities to achieve a high-energy-density secondary battery compared to Li—S and Li–air battery. Commercialized NMC with high specific capacity was employed as high-voltage cathode materials and paired with Li metal anode to construct Li | NMC cells.[26,49] FEC additive can effectively prolong the cycling life, reduce the interphase resistance and the amounts of dead Li. This contribution provides new perspective for the effect of LiF-rich SEI induced by FEC on uniform Li deposits and high Coulombic efficiency, and simultaneously exhibits the potential application of LMB with conversion-type Li metal anode and intercalation-type NMC cathode. However, the mechanism of reductive decomposition of FEC should be further probed to the dynamic role of FEC in forming stable SEI profoundly.

3. Conclusions

FEC additives were used in a working battery to achieve an LiF-rich SEI and therefore effectively protect Li metal. The first-principles calculations indicate that FEC with a very low LUMO level of –0.87 eV is very easy to reduce on the surface of Li metal anode to form LiF. The LiF-rich SEI is efficient and effective to suppress Li dendrite growth. The Coulombic efficiency of Li | Cu cells is 98% and a reduced and stable polarization of 50 mV is achieved with 5% FEC electrolyte. This affords uniform and dense morphology of deposited Li in a working cell. When the FEC-protected Li metal anode matches a high loading NMC cathode (12 mg cm^{-2}) to assemble an LMB, a high initial capacity of 154 mAh g^{-1} (1.9 mAh cm^{-2}) at 180.0 mA g^{-1} was obtained. A sharp capacity drop of cells in FEC-free electrolyte is induced by unstable interface with large dead Li covered on Li anode. The FEC-protected Li metal anode guarantees the efficient operation of LMB with long cycle life. The strategy of Li metal battery with conversion-type Li metal anode and intercalation-type NMC cathode affords an emerging energy storage system to probe the energy chemistry of Li metal protection and demonstrate the materials engineering of batteries with very high energy density. The in situ generated stable LiF-rich SEI strategy is expected to be applied in other metal batteries (e.g., Li—S, Li–air, and Zn–air batteries) with dendrite-free growth and very high Coulombic efficiency.

4. Experimental Section

Materials: Li metal foil was commercially available from China Energy Lithium Co., Ltd. The electrolyte composed of $LiPF_6$ (1.0 M) and EC/DEC (1:1 by volume) was purchased from the Beijing Institute of Chemical Reagents. FEC was purchased from Alfa Aesar. NMC cathode materials (NMC coated on Al foil) were purchased from Henan Huanyu Power Source Co., Ltd., containing 80% active material, 10% super P, and 10% polyvinylidene fluoride binder. The typical active materials loadings of cathode were about 12–14 mg cm^{-2}. All the NMC electrodes were dried under vacuum for 6 h before use.

Structure Characterizations: The morphologies of the Li metal anodes and corresponding Li deposits were characterized by SEM (JSM 7401F, JEOL Ltd., Japan) operated at 3.0 kV. An AlKα radiation (72 W, 12 kV) at a pressure of 10^{-9} Torr was applied to acquire XPS spectra on ESCALAB 250Xi (Thermo Fisher Scientific Inc., USA). The diameter of the analyzed area was 400 µm. The Li metal anodes and Li deposits on Cu foil (stripping state) sample obtained from disassembled cells were first cleaned by DEC solvent three times, and then dried until the solvent volatilized thoroughly in the glove box. During transferring process before characterizations, all samples were protected with Ar in homemade container to avoid contact with air.

Computational Details: The geometry optimization of EC, FEC, and DEC molecule was applied in DMol3 module in Materials Studio[50] (version 5.5) of Accelrys Inc. with B3LYP[51] functional. An all-electron numerical basis set with polarization functions (DNP basis set) and a basis file of 4.4 were used during the calculation. The convergence tolerance was set to be fine: 1.0×10^{-5} Ha, 2.0×10^{-3} Ha Å^{-1}, and 5.0×10^{-3} Å for energy, maximum force, and maximum displacement, respectively. The AIMD was conducted in CASTEP[52] module with general gradient approximation[53] (GGA) and Perdew–Burke–Ernzerhof[54] (PBE) exchange-correlation functional. Three models were considered here: Li-110+10EC+5DEC, Li-110+9EC+5DEC+FEC, and LiF-100+5EC+3DEC.[55] Take the model, Li-110+10EC+5DEC, as an example: Li-110 meant a seven-layer 2 × 2 supercell of lithium (110) surface with a vacuum of 1.5 nm; 10EC+5DEC meant ten EC molecules and five DEC molecules were put in the 1.5 nm vacuum simulating the electrolyte. A minimization calculation was conducted first in Discover module in Material Studio and consistent valence force field (cvff) was adopted (compass force field was adopted in LiF-100+5EC+3DEC). Then a 4.0 ps AIMD was implemented in CASTEP3 with *NVT* ensemble. The time step was set to 1.0 fs and the temperature was set to 300 K. Besides, Nose thermostat with a Nose *Q* ratio of 0.5[56] was chosen.

Electrochemical Measurement: Two-electrode cells configuration using standard 2025 coin-type cells was employed and assembled in an Ar-filled glove box with O_2 and H_2O content below 5.0 ppm. The electrolytes were prepared by adding 5% FEC additives (by volume) into 1.0 M $LiPF_6$ in EC/DEC (1:1 by volume), and then stirred for 5 h. The Cu foil and NMC electrode foil were punched into 13.0 mm disks as the working electrodes. The Li | Cu cells were cycled within a voltage range of –0.5 to 1.0 V at a current density of 0.1 and 0.5 mA cm^{-2}. In each cycle, the cells were first discharged for 1.0 h (except for 0.1 mA cm^{-2}) and then charged to the cutoff voltage of 1.0 V. The Li | NMC coin cells were monitored in galvanostatic mode within a voltage range of 3.0–4.3 V versus Li$^+$/Li using LAND multichannel battery cycler (Wuhan LAND Electronics Co., Ltd.). The Li | NMC cells were first cycled at 0.1 C for one cycle and then cycled at 1 C (≈180 mA g^{-1} based on NMC cathode materials). The EIS measurement was performed in frequency ranging from 10^5 to 10^{-1} Hz under amplitude of 10 mV using Solartron 1470E electrochemical workstation (Solartron Analytical, UK). The equivalent circuit fitted for the EIS spectra is from a previous publication.[34]

Supporting Information

Supporting Information is available from the Wiley Online Library or from the author.

Acknowledgements

X.Q.Z., X.B.C., and X.C. contributed equally to this work. This work was supported by National Key Research and Development Program (No. 2016YFA0202500) and Natural Scientific Foundation of China (Nos. 21422604, 21676160, and 21561130151). The authors thank Jia-Qi Huang, Rui Zhang, Chen-Zi Zhao, and Hong-Jie Peng at Tsinghua University for helpful discussion.

Received: November 14, 2016
Revised: December 19, 2016

---

[1] J. M. Tarascon, M. Armand, *Nature* **2001**, *414*, 359.
[2] B. Dunn, H. Kamath, J. M. Tarascon, *Science* **2011**, *334*, 928.
[3] a) M. D. Tikekar, S. Choudhury, Z. Tu, L. A. Archer, *Nat. Energy* **2016**, *1*, 16114; b) P. He, T. Zhang, J. Jiang, H. Zhou, *J. Phys. Chem. Lett.* **2016**, *7*, 1267.
[4] Y. Sun, N. Liu, Y. Cui, *Nat. Energy* **2016**, *1*, 16071.
[5] a) W. Xu, J. Wang, F. Ding, X. Chen, E. Nasybulin, Y. Zhang, J.-G. Zhang, *Energy Environ. Sci.* **2014**, *7*, 513; b) X. B. Cheng, R. Zhang, C. Z. Zhao, F. Wei, J. G. Zhang, Q. Zhang, *Adv. Sci.* **2016**, *3*, 1500213.
[6] M. Rosso, T. Gobron, C. Brissot, J. N. Chazalviel, S. Lascaud, *J. Power Sources* **2001**, *97*, 804.
[7] a) Z. Tu, P. Nath, Y. Lu, M. D. Tikekar, L. A. Archer, *Acc. Chem. Res.* **2015**, *48*, 2947; b) X. B. Cheng, T. Z. Hou, R. Zhang, H. J. Peng, C. Z. Zhao, J. Q. Huang, Q. Zhang, *Adv. Mater.* **2016**, *28*, 2888.
[8] a) R. Zhang, X. B. Cheng, C. Z. Zhao, H. J. Peng, J. L. Shi, J. Q. Huang, J. Wang, F. Wei, Q. Zhang, *Adv. Mater.* **2016**, *28*, 2155; b) C. P. Yang, Y. X. Yin, S. F. Zhang, N. W. Li, Y. G. Guo, *Nat. Commun.* **2015**, *6*, 8058.
[9] a) N. W. Li, Y. X. Yin, C. P. Yang, Y. G. Guo, *Adv. Mater.* **2016**, *28*, 1853; b) Z. Liu, Y. Qi, Y. X. Lin, L. Chen, P. Lu, L. Q. Chen, *J. Electrochem. Soc.* **2016**, *163*, A592; c) E. Peled, *J. Electrochem. Soc.* **1997**, *144*, L208.
[10] K. Xu, *Chem. Rev.* **2004**, *104*, 4303.
[11] a) V. Thangadurai, S. Narayanan, D. Pinzaru, *Chem. Soc. Rev.* **2014**, *43*, 4714; b) Y. Yamada, A. Yamada, *J. Electrochem. Soc.* **2015**, *162*, A2406; c) D. Aurbach, *Solid State Ionics* **2002**, *148*, 405; d) D. Wang, W. Zhang, W. Zheng, X. Cui, T. Rojo, Q. Zhang, *Adv. Sci.* **2016**, *3*, 1600168.
[12] K. Xu, *Chem. Rev.* **2014**, *114*, 11503.
[13] a) H. Ota, K. Shima, M. Ue, J.-I. Yamaki, *Electrochim. Acta* **2004**, *49*, 565; b) J. Guo, Z. Wen, M. Wu, J. Jin, Y. Liu, *Electrochem. Commun.* **2015**, *51*, 59.
[14] J. Heine, P. Hilbig, X. Qi, P. Niehoff, M. Winter, P. Bieker, *J. Electrochem. Soc.* **2015**, *162*, A1094.
[15] Q. C. Liu, J. J. Xu, S. Yuan, Z. W. Chang, D. Xu, Y. B. Yin, L. Li, H. X. Zhong, Y. S. Jiang, J. M. Yan, X. B. Zhang, *Adv. Mater.* **2015**, *27*, 5241.
[16] a) D. Aurbach, E. Pollak, R. Elazari, G. Salitra, C. S. Kelley, J. Affinito, *J. Electrochem. Soc.* **2009**, *156*, A694; b) S. S. Zhang, *J. Power Sources* **2016**, *322*, 99.
[17] F. Ding, W. Xu, G. L. Graff, J. Zhang, M. L. Sushko, X. Chen, Y. Shao, M. H. Engelhard, Z. Nie, J. Xiao, X. Liu, P. V. Sushko, J. Liu, J. G. Zhang, *J. Am. Chem. Soc.* **2013**, *135*, 4450.
[18] a) C. Yan, X.-B. Cheng, C.-Z. Zhao, J.-Q. Huang, S.-T. Yang, Q. Zhang, *J. Power Sources* **2016**, *327*, 212; b) W. Li, H. Yao, K. Yan, G. Zheng, Z. Liang, Y. M. Chiang, Y. Cui, *Nat. Commun.* **2015**, *6*, 7436; c) C.-Z. Zhao, X.-B. Cheng, R. Zhang, H.-J. Peng, J.-Q. Huang, R. Ran, Z.-H. Huang, F. Wei, Q. Zhang, *Energy Storage Mater.* **2016**, *3*, 77.
[19] Y. Lu, Z. Tu, J. Shu, L. A. Archer, *J. Power Sources* **2015**, *279*, 413.
[20] Y. Lu, Z. Tu, L. A. Archer, *Nat. Mater.* **2014**, *13*, 961.
[21] C. Zu, A. Dolocan, P. Xiao, S. Stauffer, G. Henkelman, A. Manthiram, *Adv. Energy Mater.* **2016**, *6*, 1501933.
[22] a) J. Qian, W. A. Henderson, W. Xu, P. Bhattacharya, M. Engelhard, O. Borodin, J. G. Zhang, *Nat. Commun.* **2015**, *6*, 6362; b) L. Suo, Y. S. Hu, H. Li, M. Armand, L. Chen, *Nat. Commun.* **2013**, *4*, 1481.
[23] a) A. Manthiram, S. H. Chung, C. X. Zu, *Adv. Mater.* **2015**, *27*, 1980; b) J.-Q. Huang, Q. Zhang, F. Wei, *Energy Storage Mater.* **2015**, *1*, 127; c) R. Cao, W. Xu, D. Lv, J. Xiao, J.-G. Zhang, *Adv. Energy Mater.* **2015**, *5*, 1402273; d) S. Zhang, K. Ueno, K. Dokko, M. Watanabe, *Adv. Energy Mater.* **2015**, *5*, 1500117; e) Q.-C. Liu, J.-J. Xu, S. Yuan, Z.-W. Chang, D. Xu, Y.-B. Yin, L. Li, H.-X. Zhong, Y.-S. Jiang, J.-M. Yan, X.-B. Zhang, *Adv. Mater.* **2015**, *27*, 5241.
[24] A. Manthiram, J. C. Knight, S.-T. Myung, S.-M. Oh, Y.-K. Sun, *Adv. Energy Mater.* **2016**, *6*, 1501010.

[25] D. Lu, Y. Shao, T. Lozano, W. D. Bennett, G. L. Graff, B. Polzin, J. Zhang, M. H. Engelhard, N. T. Saenz, W. A. Henderson, P. Bhattacharya, J. Liu, J. Xiao, *Adv. Energy Mater.* **2015**, *5*, 1400993.

[26] J. Zheng, P. Yan, D. Mei, M. H. Engelhard, S. S. Cartmell, B. J. Polzin, C. Wang, J.-G. Zhang, W. Xu, *Adv. Energy Mater.* **2016**, *6*, 1502151.

[27] A. M. Haregewoin, A. S. Wotango, B.-J. Hwang, *Energy Environ. Sci.* **2016**, *9*, 1955.

[28] D. Y. Wang, N. N. Sinha, J. C. Burns, C. P. Aiken, R. Petibon, J. R. Dahn, *J. Electrochem. Soc.* **2014**, *161*, A467.

[29] a) V. Etacheri, O. Haik, Y. Goffer, G. A. Roberts, I. C. Stefan, R. Fasching, D. Aurbach, *Langmuir* **2012**, *28*, 965; b) C. Xu, F. Lindgren, B. Philippe, M. Gorgoi, F. Björefors, K. Edström, T. Gustafsson, *Chem. Mater.* **2015**, *27*, 2591.

[30] E. Markevich, G. Salitra, K. Fridman, R. Sharabi, G. Gershinsky, A. Garsuch, G. Semrau, M. A. Schmidt, D. Aurbach, *Langmuir* **2014**, *30*, 7414.

[31] Y. Li, F. Lian, L. L. Ma, C. L. Liu, L. Yang, X. M. Sun, K. C. Chou, *Electrochim. Acta* **2015**, *168*, 261.

[32] J. Pan, Y.-T. Cheng, Y. Qi, *Phys. Rev. B* **2015**, *91*, 134116.

[33] a) L. Chen, H. W. Zhang, L. Y. Liang, Z. Liu, Y. Qi, P. Lu, J. Chen, L.-Q. Chen, *J. Power Sources* **2015**, *300*, 376; b) H. Xiang, P. Shi, P. Bhattacharya, X. Chen, D. Mei, M. E. Bowden, J. Zheng, J.-G. Zhang, W. Xu, *J. Power Sources* **2016**, *318*, 170.

[34] X. B. Cheng, H. J. Peng, J. Q. Huang, R. Zhang, C. Z. Zhao, Q. Zhang, *ACS Nano* **2015**, *9*, 6373.

[35] a) G. Deniz, L.-W. Kendra, S. Ravishankar, A. S. Kathleen, T. A. Arias, *Model. Simul. Mater. Sci.* **2013**, *21*, 074005; b) A. L. Michan, B. S. Parimalam, M. Leskes, R. N. Kerber, T. Yoon, C. P. Grey, B. L. Lucht, *Chem. Mater.* **2016**, *28*, 8149.

[36] M. Y. Nie, J. Demeaux, B. T. Young, D. R. Heskett, Y. J. Chen, A. Bose, J. C. Woicik, B. L. Lucht, *J. Electrochem. Soc.* **2015**, *162*, A7008.

[37] a) M. Sina, J. Alvarado, H. Shobukawa, C. Alexander, V. Manichev, L. Feldman, T. Gustafsson, K. J. Stevenson, Y. S. Meng, *Adv. Mater. Interfaces* **2016**, *3*, 1600438; b) X. Chen, X. Li, D. Mei, J. Feng, M. Y. Hu, J. Hu, M. Engelhard, J. Zheng, W. Xu, J. Xiao, J. Liu, J.-G. Zhang, *ChemSusChem* **2014**, *7*, 549.

[38] a) S. Komaba, T. Ishikawa, N. Yabuuchi, W. Murata, A. Ito, Y. Ohsawa, *ACS Appl. Mater. Interfaces* **2011**, *3*, 4165; b) M. Kohl, F. Borrmann, H. Althues, S. Kaskel, *Adv. Energy Mater.* **2016**, *6*, 1502185.

[39] N. Wang, Y. Gao, Y.-X. Wang, K. Liu, W. Lai, Y. Hu, Y. Zhao, S.-L. Chou, L. Jiang, *Adv. Sci.* **2016**, *3*, 1600013.

[40] W. Li, S.-L. Chou, J.-Z. Wang, J. H. Kim, H.-K. Liu, S.-X. Dou, *Adv. Mater.* **2014**, *26*, 4037.

[41] a) Z. Li, J. Huang, B. Y. Liaw, V. Metzler, J. Zhang, *J. Power Sources* **2014**, *254*, 168; b) Z. Zeng, X. Jiang, R. Li, D. Yuan, X. Ai, H. Yang, Y. Cao, *Adv. Sci.* **2016**, *3*, 1600066.

[42] S. Hong, M.-H. Choo, Y. H. Kwon, J. Y. Kim, S.-W. Song, *Adv. Mater. Interfaces* **2016**, *3*, 1600172.

[43] I. A. Shkrob, J. F. Wishart, D. P. Abraham, *J. Phys. Chem. C* **2015**, *119*, 14954.

[44] Z. Yang, A. A. Gewirth, L. Trahey, *ACS Appl. Mater. Interfaces* **2015**, *7*, 6557.

[45] J. Wang, C. Luo, T. Gao, A. Langrock, A. C. Mignerey, C. Wang, *Small* **2015**, *11*, 473.

[46] L. Suo, O. Borodin, T. Gao, M. Olguin, J. Ho, X. Fan, C. Luo, C. Wang, K. Xu, *Science* **2015**, *350*, 938.

[47] K. Kanamura, S. Shiraishi, Z. i. Takehara, *J. Electrochem. Soc.* **1996**, *143*, 2187.

[48] a) S. S. Zhang, *J. Power Sources* **2006**, *162*, 1379; b) F. Ding, W. Xu, X. Chen, J. Zhang, M. H. Engelhard, Y. Zhang, B. R. Johnson, J. V. Crum, T. A. Blake, X. Liu, J. G. Zhang, *J. Electrochem. Soc.* **2013**, *160*, A1894.

[49] S. Choudhury, L. A. Archer, *Adv. Electron. Mater.* **2016**, *2*, 1500246.

[50] a) B. Delley, *J. Chem. Phys.* **1990**, *92*, 508; b) B. Delley, *J. Chem. Phys.* **2000**, *113*, 7756.

[51] A. D. Becke, *J. Chem. Phys.* **1993**, *98*, 5648.

[52] S. J. Clark, M. D. Segall, C. J. Pickard, P. J. Hasnip, M. I. J. Probert, K. Refson, M. C. Payne, *Z. Kristallogr. - Cryst. Mater.* **2005**, *220*, 567.

[53] Y. Zhou, C. Zhou, Q. Li, C. Yan, B. Han, K. Xia, Q. Gao, J. Wu, *Adv. Mater.* **2015**, *27*, 3774.

[54] J. P. Perdew, K. Burke, M. Ernzerhof, *Phys. Rev. Lett.* **1996**, *77*, 3865.

[55] K. Gaedt, H. D. Höltje, *J. Comput. Chem.* **1998**, *19*, 935.

[56] S. I. Nosé, *Mol. Phys.* **2002**, *100*, 191.